IP-3 | 1227

MILITARY TECHNICAL COLLEGE
CAIRO - EGYPT

RECONSTRUCTION OF DIGITAL IMAGES FROM PROJECTIONS

M.ELYOUNSI + A.SHAHIN ++

ABSTRACT

This paper has applied the mathematical process of reconstruction of a three dimensional objects as used in Computer Axial Tomography (CAT). It uses direct convolution techniques with functions defined in the real space of the object either with parallel projections or with fan-beam projections.

The simulated data is obtained using a disk having a uniform density from the centre up to radius equal 0.8 except for an off centre hump, beyond which it tends smoothly to zero if the radius equals 1.2 . The data has been simulated at different sample intervals and different projection angles .

The reconstructed image by using the convolution techniques with two types of filters for parallel ray and fan-beam has acceptable error that does not exceed 2% at greater number of projections and smaller sampling interval .

INTRODUCTION :

The digital reconstruction techniques for an image from its projections has become important during the past few years. The significance of these techniques is manifisted from their applications to areas such as medical radiology and nuclear medicine, electron microscopy, radio and radar astronomy, light microscopy and holography. The algorithms of these techniques have extended our ability to visualize the internal structures of objects. These algorithms are applicable when the measured data has the form of line or strip integrals of the spatial distribution of a physical property of interest [1-2]. In computerized tomography (CT) where X-rays are used to generate the projection data for a cross-section of the human body, the reconstructed image is obtained with many morphological details of the body in that cross-section .

There are a number of different approaches for the reconstruction, namely, the Fourier techniques [3], the convolution method [4-6], and the algebric techniques [7].

+ Graduated Student, ++Head of A/C Elect. Equip. Dept. MTC.

The scope of this paper deals with the evaluation of the convolution algorithms for reconstruction of a two-dimenstional (2-D) image using projections from parallel and fan-beam geometry .

First section, discusses the reconstruction of images by convolution techniques using two types of filters in order to convolve the parallel projection data. In second section, the convolution algorithms using the two filters are adapted for image reconstruction from the fan-beam projection data. Third section, presents the flowchart of the convolution algorithms and its implementation to reconstruct a disk that has three regions of density variations. The simulated data are obtained from the parallel and the fan-beam geometry at different number of projections and different sampling intervals. The accuracy of the reconstructed disk using different types of filters are studied, and the comparison between the actual and reconstructed values are presented .

1 . PARALLEL RAYS RECONSTRUCTION BY CONVOLUTION AND BACK-PROJECTION

The object which is usually represented by its linear attenuation coefficient $f(x,y)$, is scanned by a source-detector arrangement [8-9] . The attenuation coefficient of the object is integrated over the ray path in Fig.1. The object is scanned by parallel rays with sampling interval a ,so that a set of parallel projections is generated. Each measurement value of one set $g(s_m,\theta_j)$ is defined by the distance s_m, of the corresponding ray path from the centre; $s_m = ma$, $m = -M/2,\ldots,0,\ldots,M/2$;which is equivalent to the position of the detector. The sets of parallel projections differ according to the tilting angle θ_j, $j = 1,\ldots,N$. The variable "s" describes a rotating coordinate defined by ,

$$\begin{bmatrix} s \\ t \end{bmatrix} = \begin{bmatrix} \cos\theta & \sin\theta \\ -\sin\theta & \cos\theta \end{bmatrix} \begin{bmatrix} x \\ y \end{bmatrix} \qquad (1.1)$$

which tracks the tilting angle θ .
The projection data $g(s,\theta)$ is the integral of $f(x,y)$ along the ray $L(s,\theta)$

$$g(s,\theta) = \int_{L(s,\theta)} f(x,y)\ dt \qquad (1.2)$$

where the line $L(s,\theta)$ is represented by $x\cos\theta + y\sin\theta = s$,and the Fourier transform (F.T.) of the projection data is ;

$$F(R,\theta) = \int_{-\infty}^{\infty} g(s,\theta) \exp(-2\pi jRs)\ ds \qquad (1.3)$$

From Eqs. (1.2) and (1.3) ,therefore ;

$$F(R,\theta) = \iint_{-\infty}^{\infty} f(x,y) \exp[-2\pi jR(x\cos\theta + y\sin\theta)]\ dx\,dy \qquad (1.4)$$

Then ,

$$f(x,y) = \int_0^{\pi} d\theta \int_{-\infty}^{\infty} |R|\, F(R,\theta) \exp[2\pi jR(x\cos\theta + y\sin\theta)]\ dR \qquad (1.5)$$

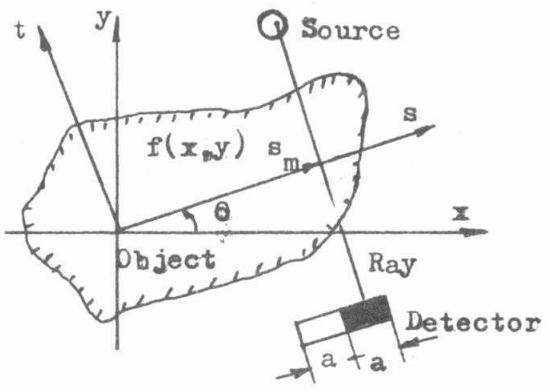

FIG. 1 . Geometric arrangement of a scanning unit generating parallel ray projection .

The inner integral of (1.5) is defined as,

$$b(s,\theta) = \int_{-\infty}^{\infty} |R|\ F(R,\theta) \exp(2\pi jRs)\ dR \qquad (1.6)$$

where, $b(s,\theta)$ is called the back-projection formula ;and

$$f(x,y) = \int_{0}^{\pi} b(x\cos\theta + y\sin\theta)\ d\theta \qquad (1.7)$$

By the convolution property of F.T. the filtered projection is

$$b(s,\theta) = \int_{-\infty}^{\infty} g(s_1,\theta)\ q(s - s_1)\ ds_1 \qquad (1.8)$$

where $g(s,\theta)$ and $q(s)$ are the inverse F.T. of $F(R,\theta)$ and $|R|$ respectively hence ,

$$q(s) = \int_{-\infty}^{\infty} |R| \exp(2\pi jRs)\ dR \qquad (1.9)$$

If $f(x,y)$ is bounded by $-T/2 \le x,y \le T/2$,then $g(s,\theta)$ is spatially limited to the interval $(-T/2\ ,T/2)$ i.e. $|s| < T/2$ .If the projection data $g(s,\theta)$ are measured at a set of equally spaced points $s=ma$, $-M/2 \le m \le M/2$;then

$$b(na,\theta) = a \sum_{m=-M/2}^{M/2} g(ma,\theta)\ q(n - m)a \qquad (1.10)$$

The accuracy of reconstruction depends greatly upon the filter $q(s)$ [4-6], [10] . The $|R|$ response is approximated within the frequency interval $(-w,w)$, in this case ;

$$q(s) = \int_{-w}^{w} |R| \exp(2\pi jRs)\ dR \qquad (1.11)$$

According to the sampling theorem [11] ,the upper frequency limit (w) of the reconstructed image sampled with a sampling interval "a" ;is

$$w = 1/2a \qquad (1.12)$$

Thus the samples, $q(na)$, of $q(s)$ are represented by two cases ,

First Case :

$$q_1(na) = \begin{cases} 1/4a^2 & n = 0 \\ 0 & n \text{ even} \\ -1/(na)^2 & n \text{ odd} \end{cases} \qquad (1.13)$$

$$b_1(na,\theta) = g(na,\theta)/4a - \frac{1}{\pi^2 a} \sum_{\text{podd}} g[(n+p)a,\theta]/p^2 \qquad (1.14)$$

Secod Case :

. Shepp and Logan [5] had modified the above filter function to be

$$q_2(na) = \begin{cases} 2/(\pi a)^2 & n = 0 \\ -2/(\pi a)^2(4n^2-1) & n = \pm 1,..... \end{cases} \qquad (1.15)$$

This filter is used as a convolving function in Eq. (1.10)

$$b_2(na,\theta) = -2/\pi^2 a \sum_{m=-M/2}^{M/2} g(ma,\theta) / [4(n - m)^2 - 1] \qquad (1.16)$$

Finally, the reconstructed image is

$$f(x,y) = \pi/N \sum_{j=1}^{N} b(x\cos\theta_j + y\sin\theta_j) \qquad (1.17)$$

where,

$\theta_j = j\pi/N$, and N is the total number of scans sampled uniformly between zero and π. The linear interpolation is used to calculate the value of $b(x\cos\theta_j + y\sin\theta_j)$ in Eq. (1.17) from the pre-calculated values of $b(na,\theta)$.

2 . FAN-BEAM RECONSTRUCTION BY CONVOLUTION AND BACK-PROJECTION

The new scanning systems generate the different sampling points of one projection simultaneously by means of a detector array [12-14] in order to reduce the excessive scanning time which is mainly caused by the mechanical shift of a single detector. This is achieved by using a fan-beam of rays which diverge from a source moving in a circular path arround the object. The rays which pass through the object are intercepted by an array of detector elements Fig. 2.

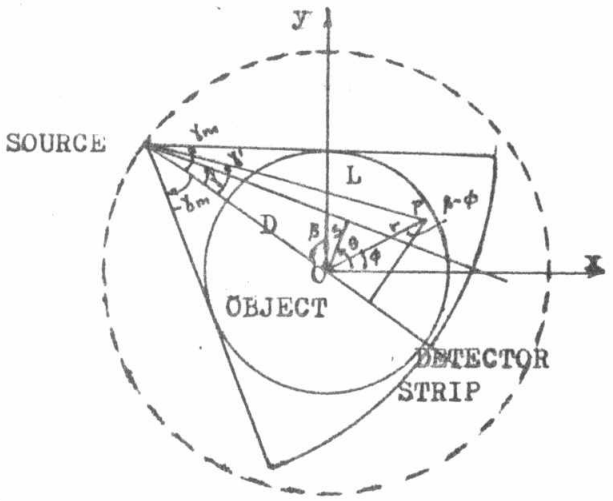

FIG. 2. Fan-beam geometry with its various parameters .

2.1. Adaptation of the Parallel-Ray for the Fan-Beam Geometry :

The projection data generated by the fan-beam along ray (γ,β) is denoted by $R(\gamma,\beta)$, where γ gives the location of a ray within the fan and β determines the source position Fig. 2. The relationships between the parallel and divergent rays geometry are ,

$$s = D \sin\gamma \quad , \quad \theta = \gamma + \beta \quad , \quad g(s,\theta) = R(\gamma,\beta) \qquad (2.1)$$

where, D is the distance of the source from the origin O .
In the preceeding section, from parallel projections $g(s,\theta)$ collected over 180°, $f(x,y)$ is reconstructed by Eqs. (1.7) and (1.8). However, when the projections are generated over 360°, these equations can be rewritten as;

$$f(x,y) = \tfrac{1}{2} \int_0^{2\pi} \int_{-s_m}^{s_m} g(s,\theta)\, q(x\cos\theta + y\sin\theta - s)\, ds\, d\theta \qquad (2.2)$$

and in polar coordinates (r,ϕ) , as

$$f(r,\phi) = \tfrac{1}{2} \int_0^{2\pi} \int_{-s_m}^{s_m} g(s,\theta)\, q(r\cos(\theta-\phi) - s)\, ds\, d\theta \qquad (2.3)$$

where , s_m is the value of s for which $g(s,\theta) = 0$ for $|s| > s_m$. The variables in (2.3) are change by the relationships in (2.1) then ,

$$f(r,\phi) = \tfrac{1}{2} \int_{-\delta}^{2\pi-\delta} \int_{-\gamma_m}^{\gamma_m} R(\gamma,\beta)\, q(r\cos(\beta+\gamma-\phi) - D\sin\gamma)\, D\cos\gamma\, d\gamma\, d\beta \qquad (2.4)$$

where ,

$$ds\, d\theta = D\cos\gamma\, d\gamma\, d\beta \quad , \quad \gamma_m = \sin^{-1}(s_m/D) \; ; \; 0 < \gamma_m < \pi/2 \qquad (2.5)$$

In Eq. (2.4) the integrand is periodic of period 2π w.r.t.β, then the limits of the β-integration is replaced by 0 and 2π. The argument of q is written as ,

$$r\cos(\beta+\gamma-\phi) - D\sin\gamma = r\cos(\beta-\gamma)\cos\gamma - (r\sin(\beta-\phi)+D)\sin\gamma \qquad (2.6)$$

The following relationships are evident from Fig. 2 ;

$$L\cos\gamma' = D + r\sin(\beta-\phi) \quad , \quad L\sin\gamma' = r\cos(\beta-\phi) \qquad (2.7)$$

and

$$L^2(r,\phi,\beta) = (D + r\sin(\beta-\phi))^2 + (r\cos(\beta-\phi))^2 \; ; \qquad (2.8)$$

$$\gamma' = \tan^{-1}\left(r\cos(\beta-\phi) / D + r\sin(\beta-\phi) \right)$$

where, L is the distance from the source to a point (r,ϕ) and γ' is the angle of that ray passes through this point. From Eqs. (2.4),(2.6) and (2.7) it follows :

$$f(r,\phi) = \tfrac{1}{2} \int_0^{2\pi} \int_{-\gamma_m}^{\gamma_m} R(\gamma,\beta)\, q(L\sin(\gamma'-\gamma))\, D\cos\gamma\, d\gamma\, d\beta \qquad (2.9)$$

From Eq.(1.8) the function $q(L\sin(\gamma'-\gamma))$ written as ;

$$q(L\sin(\gamma'-\gamma)) = \int_{-\infty}^{\infty} R\, \exp(2\pi jRL\sin(\gamma'-\gamma))\, dR \qquad (2.10)$$

for ,

$$w = RL\sin(\gamma'-\gamma) / (\gamma'-\gamma)$$

$$q(L\sin(\gamma'-\gamma)) = \left(\frac{\gamma'-\gamma}{L\sin(\gamma'-\gamma)}\right)^2 \int_{-\infty}^{\infty} w\cdot \exp(2\pi jw(\gamma'-\gamma))\, dw$$

$$= \left(\frac{\gamma'-\gamma}{L\sin(\gamma'-\gamma)}\right)^2 q(\gamma'-\gamma) \qquad (2.11)$$

Therefore, Eq.(2.9) is written as ,

$$f(r,\phi) = \int_0^{2\pi} 1/L^2 \int_{-\gamma_m}^{\gamma_m} R(\gamma,\beta)\, h(\gamma'-\gamma)\, D\cos\gamma\, d\gamma\, d\beta \qquad (2.12)$$

where , $h(\gamma'-\gamma) = \tfrac{1}{2}\left(\frac{\gamma'-\gamma}{\sin(\gamma'-\gamma)}\right)^2 q(\gamma'-\gamma)$ (2.13)

The inner integral in (2.12) is defined by ,

$$Q(\gamma',\beta) = \int_{-\gamma_m}^{\gamma_m} p(\gamma,\beta)\, h(\gamma'-\gamma)\, d\gamma \qquad (2.14)$$

where, $p(\gamma,\beta) = R(\gamma,\beta)\, D\cos\gamma$ (2.15)

Hence , the reconstructed function is

$$f(r,\phi) = \int_0^{2\pi} (1/L^2)\, Q(\gamma',\beta)\, d\beta \qquad (2.16)$$

For the projection data $R(\gamma,\beta)$ sampled with interval α the reconstruction formulas (2.14) , (2.15), and(2.16) are written in discrete version as ;

$$Q(n\alpha,\beta) = \alpha \sum_{m=-M/2}^{M/2} p(m\alpha,\beta)\, h(m-n)\alpha \quad ; \quad -M/2 \le n \le M/2 \qquad (2.17)$$

$$p(m\alpha,\beta) = R(m\alpha,\beta).\, D\cos m\alpha \quad ; \quad -M/2 \le m \le M/2 \qquad (2.18)$$

$$f(x,y) = 2\pi/N \sum_{i=1}^{N} \frac{1}{L^2(x,y,\beta_i)}\, Q(\gamma',\beta_i) \qquad (2.19)$$

where ,

N is the number of projections at which the angles β_i are taken .

2.2. Filter Adaptation for Fan-Beam Geometry :

The two filter functions presented in the preceeding section are adapted for fan-beam geometry. By analogy with Eq. (1.13) ,the samples $q(n\alpha)$ of $q(\gamma)$ sampled with interval α is ;

Third Case :

$$q_A(n\alpha) = \begin{cases} 1/4\alpha^2 & n = 0 \\ 0 & n \text{ even} \\ -1/(\pi n\alpha)^2 & n \text{ odd} \end{cases} \qquad (2.20)$$

From Eqs. (2.13) and (2.20) , the adapted discrete impulse response of the filter is ;

$$h_1(n\alpha) = \begin{cases} 1/8\alpha^2 & n = 0 \\ 0 & n \text{ even} \\ -\tfrac{1}{2}(\alpha/\pi\alpha\sin n\alpha)^2 & n \text{ odd} \end{cases} \qquad (2.21)$$

$$Q_1(n\alpha,\beta) = (p(n\alpha,\beta))/8\alpha - \alpha D/2\pi^2 \sum_{k\,odd} p((k+n)\alpha,\beta)/\sin^2 k\alpha \qquad (2.22)$$

Fourth Case :

By analogy with Eq. (1.15)

$$q_B(n\alpha) = \begin{cases} 2/(\pi\alpha)^2 & n = 0 \\ -2/(\pi\alpha)^2 (4n^2 - 1) & n = \pm 1, \ldots \end{cases} \quad (2.23)$$

From Eqs. (2.13), and (2.23) the adapted filter for fan-beam geometry sampled with interval is,

$$h_2(n\alpha) = \begin{cases} 1/(\pi\alpha)^2 & n = 0 \\ -\left(\frac{n\alpha}{\pi\alpha \sin n\alpha}\right)^2 / (4n^2 - 1) & n = \pm 1, \ldots \end{cases} \quad (2.24)$$

$$Q_2(n\alpha, \beta) = 1/\pi^2\alpha\left(p(n\alpha,\beta) - \alpha^2 \sum_{\substack{k=-M/2 \\ k \neq 0}}^{M/2} p(n+k)\alpha,\beta) \cdot \frac{k^2}{(4k^2-1)\sin^2 k\alpha}\right) \quad (2.25)$$

where , $k = m - n$

The linear interpolation is used to calculate the values of $Q(\gamma', \beta)$ from the precalculated values of $Q(n\alpha, \beta)$.

3 . FLOWCHART OF ALGORITHMS AND IMPLEMENTATION :

The convolution algorithms for reconstruction an image from parallel and fan-beam are summarized in the flowcharts shown in figures 3 and 4, respectively. In order to study the algorithms efficiency and also to test if the convolution algorithms are capable of revealing a fairly localized small density change in a flat region, the object chosen is represented in Fig. 5. The object data are represented as $f(x,y)$ in matrix form with dimension (kxk). The Fig. 3 is applicable for parallel ray reconstruction at different sampling intervals "a" and different angular intervals ($\theta_o = \pi/N$) while Fig. 4 is adapted for fan-beam reconstruction at different angular intervals ($\beta_o = 2\pi/N$) , where N is the number of projections .

The reconstruction from the parallel ray has been applied using two types of filters for different number of projections 3, 6, or 12 with angular intervals θ=60°, 30°, and 15° respectively, at sampling intervals a = 0.1, and 0.2 . Also, the fan-beam has been applied using the two adapted filters for different number of projections 6, 12, or 24 with angular intervals β_o = 60°, 30°, and 15° respectively, at sampling intervals α = 1°, and 2° for each projection .

The accuracy of reconstruction was estimated through the values of the mean relative error, R_v, and the root mean square error, R_m .For parallel ray and fan-beam , these values have been calculated at different regions of the disk by utilizing the reconstructed quantities for each case according to the filter type as shown in tables 1, and 2 respectively. The error values are acceptable for greater number of projections ; and increase whenever less projections are used, specially at the variable region (V). Also, the accracy has been improved for smaller sampling intervals. The comparison between the original and the reconstructed values from parallel ray (at a=0.1 and θ_o=15°), and fan-beam (at α=1° and β_o=15°) using the corresponding filter type are shown in figures 6 and 7 respectively, where the reconstruction is quite good .

Generally, the reconstruction obtained from parallel ray or fan-beam geometry using the second filter type has better accuracy for the uniform region (U) than the first filter type which has better accuracy in the varying region (V) and near the hump (H), this can be seen in figures 8 and 9 respectively.

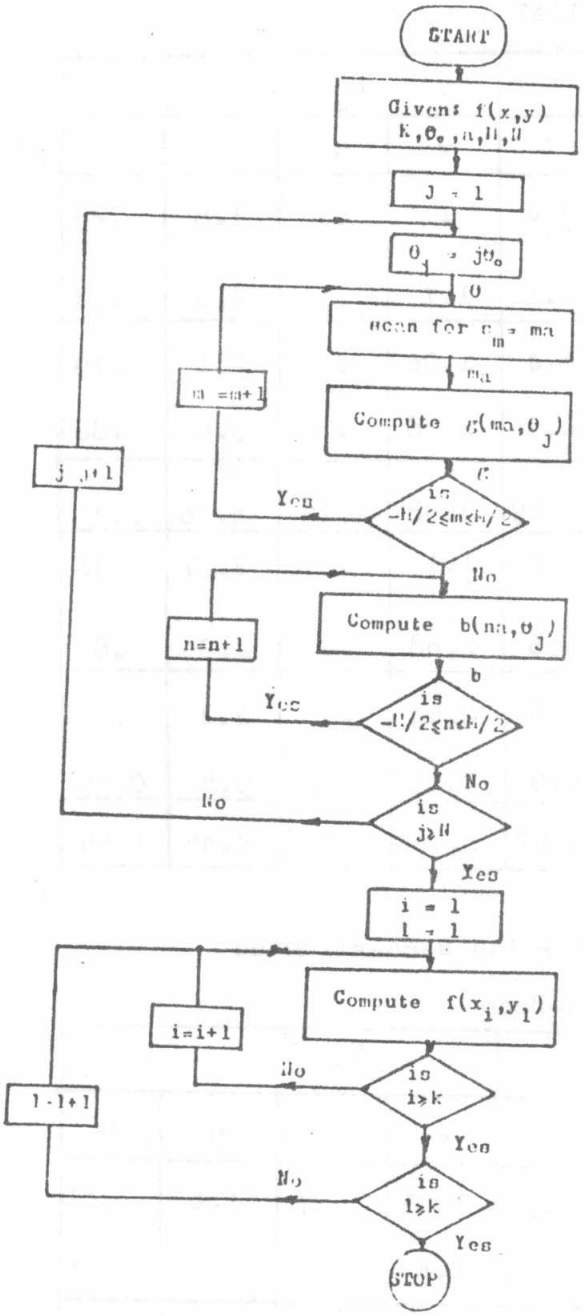

FIG. 3 Flowchart for parallel rays reconstruction

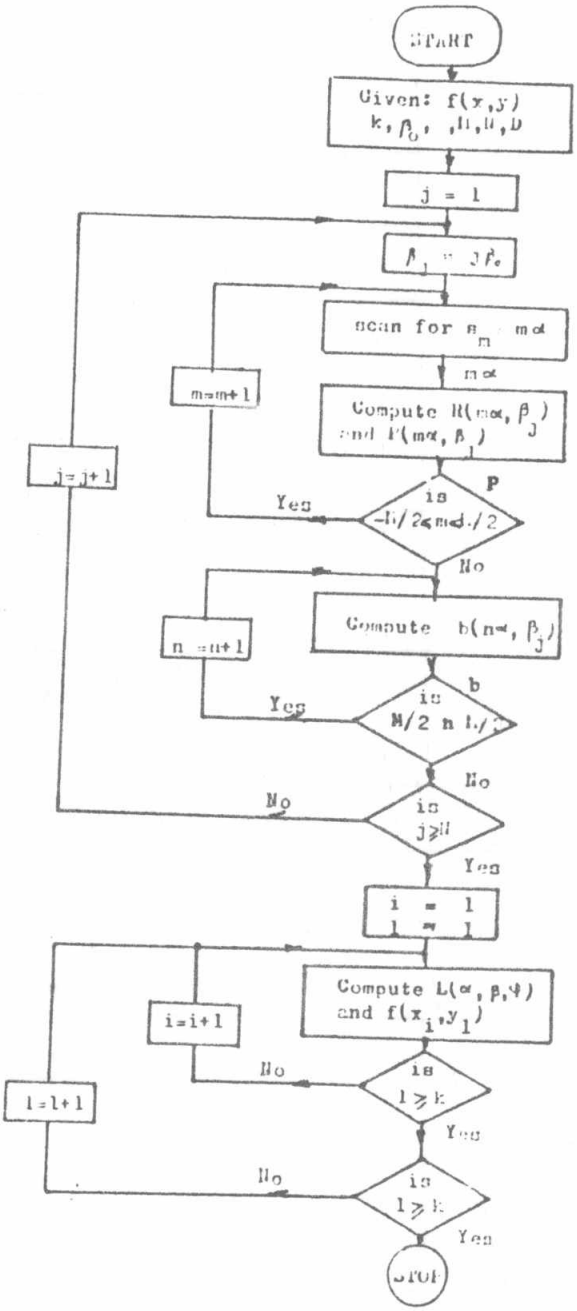

FIG. 4 Flowchart for Fan-beam reconstruction

FIG. 5 Schematic diagram of the three regions of density variations in the reconstructed object (D) .

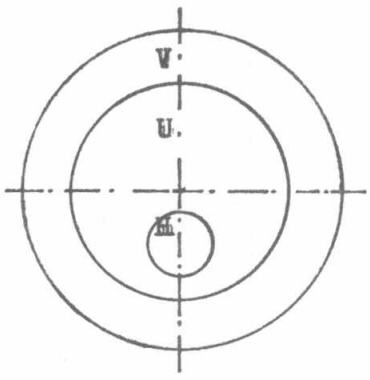

Table 1. R_v and R_m Values for the reconstructed Disk (D) using Parallel Ray

used Filter	θ	a	R_v %				R_m %			
			v	u	H	D	v	u	H	D
q_1 (case1)	15°	0.1	6.1	1.7	2.6	3.4	1	.3	1.6	.43
		0.2	11.4	2.7	6.2	6.1	1.7	.53	4.8	.74
	30°	0.1	12.5	2.59	3.5	6.4	1.96	.52	2.1	.79
		0.2	13.3	3.07	4.8	6.9	2.18	.54	3.6	.88
	60°	0.1	25.5	5.59	6.62	12.89	3.98	1.12	4.38	1.7
q_2 (case2)	15°	0.1	7.2	1.5	3.3	3.7	1.1	.3	2.37	.46
		0.2	12.7	2.8	6.1	6.6	2.08	.6	4.9	.8
	30°	0.1	11.7	2.49	4.12	6.4	2.04	.5	2.4	.74
		0.2	13.3	2.9	7.2	6.9	2.17	.57	5.8	0.89
	60°	0.1	24.03	4.65	6.67	11.52	3.79	.93	4.45	1.55

Table 2 R_v and R_m Values for the Reconstructed Disk (D) using Fan-Beam .

used Filter			R_v %				R_m %			
			v	u	H	D	v	u	H	D
h_1 (case3)	15°	1°	7.26	1.2	2.38	3.5	1.05	.27	1.6	.43
		2°	9.6	1.4	4	4.59	1.4	.34	3	.57
	30°	1°	10.79	2.1	3.16	5.2	1.68	.42	2.18	.69
		2°	11.5	2.79	5.07	5.5	1.8	.54	3.4	.72
	60°	1°	17.86	6.08	5.26	10.4	2.78	1.25	4.5	1.28
h_2 (case4)	15°	1°	7.56	1.08	2.78	2.56	1.08	.23	2.05	.43
		2°	10.95	1.54	5	5.19	1.58	.37	3.9	.65
	30°	1°	11.3	2.09	3.5	5.4	1.8	.41	2.3	.72
		2°	11.56	2.0	5.6	5.9	1.89	.5	4.1	.76
	60°	1°	17.88	5.81	5.7	10.2	2.77	1.17	3.84	1.25

4						
6.2						
7						
44	38	21	6			
46.3	35.2	24.2	5.1			
46.1	35.8	24.7	5.9			
100	98	83	44	11		
98.6	95	79	48.7	21.9		
96.8	93.4	77.5	48.2	20.9		
100	100	100	95	44	6	
103.4	101	99.6	93.1	47.9	7.8	
102.6	100.4	98.6	90.5	47.4	8.3	
100	100	100	100	83	21	
103.5	100.3	101.8	100	79.1	22	
102.7	100.1	101.1	98.9	78.1	22.8	
100	100	100	100	98	38	
102.2	101.5	100.3	101.8	96	37.8	
101.5	100.9	100	101.1	94.3	38.1	
100	100	100	100	100	44	4
106.6	100.7	102.9	101.8	96	42.8	0
104.9	100.2	102.2	101.3	94.6	43.1	0
105	100	100	100	98	38	
107.4	102.2	99.8	100.9	96.7	36.5	
107.1	101.9	99.6	100.4	94.8	37	
140	105	100	100	83	21	
135.3	107	103.5	101.4	79.8	24.5	
132.2	106.8	102.7	100	78.2	24.9	
105	100	100	95	44	6	
108.1	101.9	99.7	91.8	48	5.9	
107.7	101.5	98.6	89.4	47.9	6.6	
100	98	83	44	11		
97.1	96	79	48.7	22.1		
95.7	94.2	77.5	48.2	21		
44	38	21	6			
44.9	36.7	22.6	6.7			
44.8	37.2	23.3	7.3			
4						
C.						
O						

FIG. 6 . Reconstructed results from parallel rays (a =0.1 , O=15°)

True densities (Row I), reconstructed densities using filters

given by case 1; and case 2 (Rows II and III, respectively) .

4						
8.3						
8.1						
44	38	21	6			
50.7	38.3	24.5	7.1			
50.1	38.4	24.7	6.9			
100	98	83	44	11		
101.5	93.1	79.4	49.8	18.1		
100.4	92.3	78.7	49.3	17.6		
100	100	100	95	44	6	
103.9	100	97.6	91.1	48.8	7.1	
103.2	100.1	97.6	90.1	48.3	6.9	
100	100	100	100	83	21	
103.1	100	100.3	98.4	79.8	23.9	
102.4	99.9	99.9	98.4	79.2	24.1	
100	100	100	100	98	38	
102.2	99.8	99.4	99.1	94.5	39.2	
101.5	100	99.4	99.4	93.6	39.4	
100	100	100	100	100	44	4
107.8	100.8	101.1	100.8	97.1	47.6	0
105.4	100.4	100.7	100.5	96.4	47.4	0
105	100	100	100	98	38	
107.8	100.2	99.4	99.3	92.8	39.2	
107.3	100.6	99.4	99.5	92.1	39.3	
140	105	100	100	83	21	
135	105.5	99.8	98.3	79.5	22	
133.3	105.6	99.5	98.3	78.9	22.3	
105	100	100	95	44	6	
108	99.8	98.8	91.5	47.2	8.7	
107.6	100.2	98.7	90.4	46.8	8.4	
100	98	83	44	11		
99.7	93.5	80.3	47.5	20		
98.7	92.7	79.7	47.1	19.5		
44	38	21	6			
47.1	40.3	24.6	7.6			
46.6	40.4	24.8	7.4			
4						
0						
0						

FIG. 7 . Reconstructed results from fan-beam ($\alpha = 1^\circ$, $\beta_m = 15^\circ$)
True densities (Row), reconstructed densities using filters
given by case 3; and case 4 (Rows II and III, respectively).

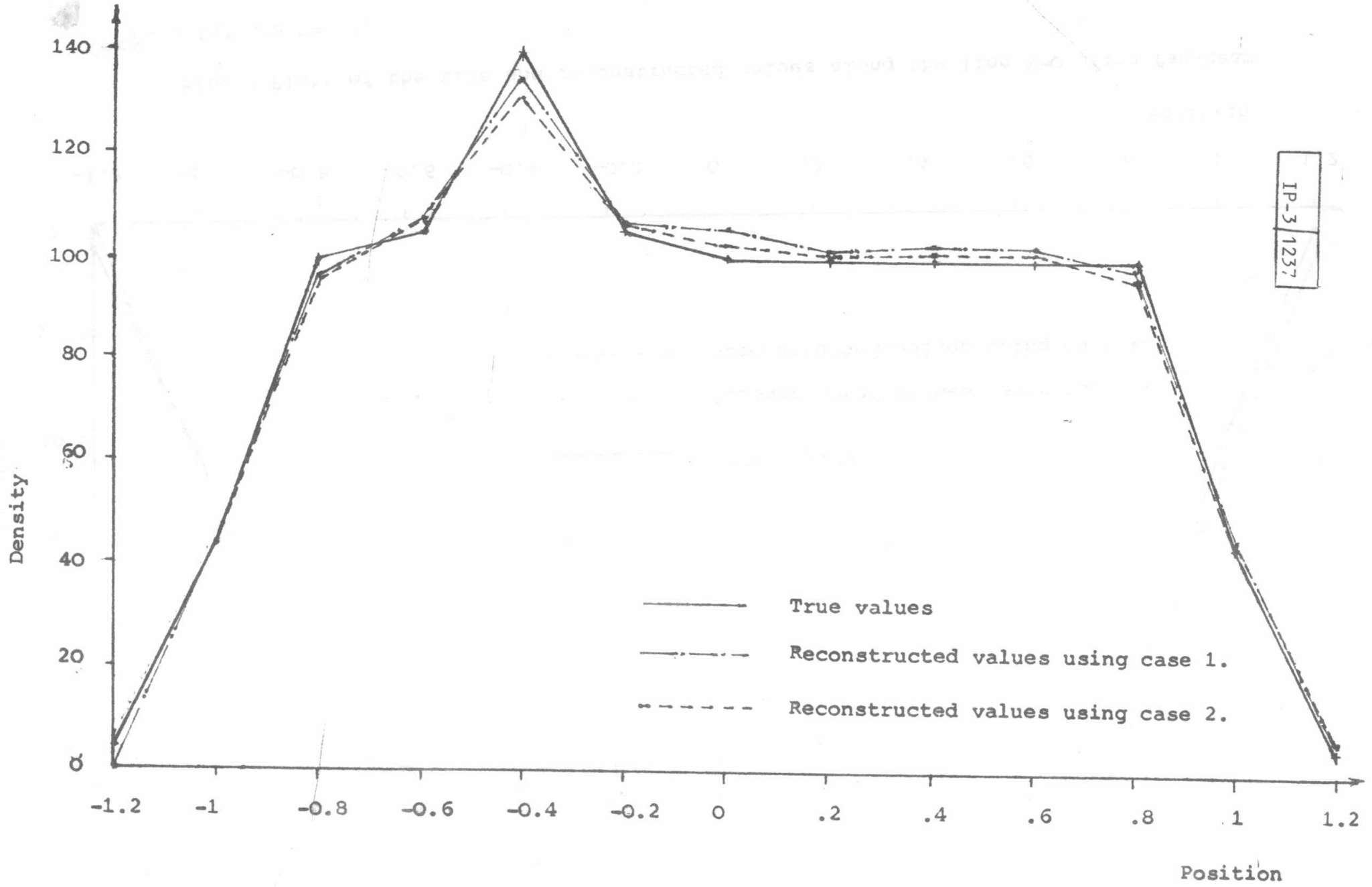

Fig. 8 Plots of the true and reconstructed values along the line X-O in using parallel for $\theta_o = 15°$ and a = 0.1.

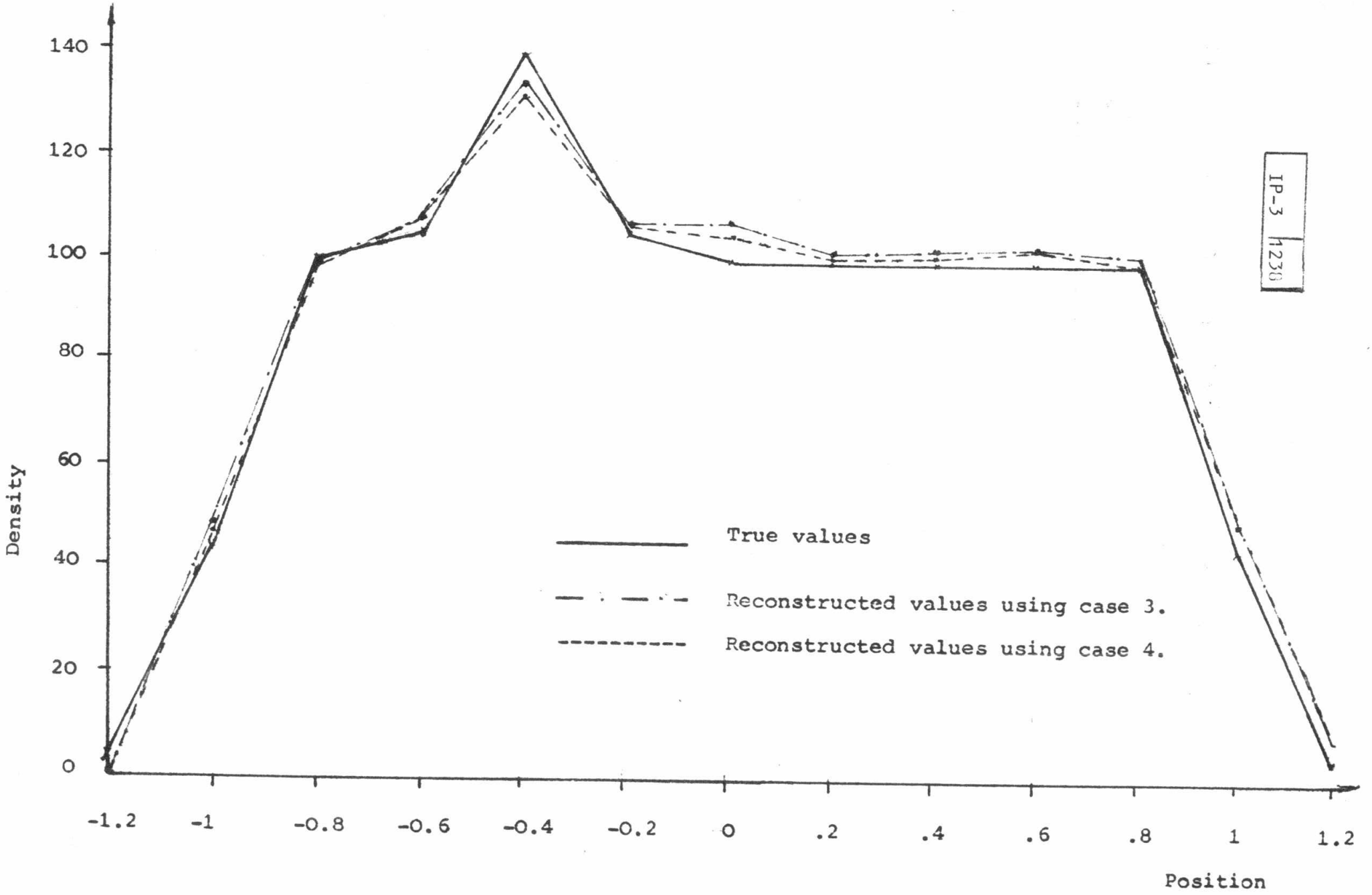

Fig. 9 Plots of the true and reconstructed values along the line X=0 using fan-beam for $\beta_0 = 15°$ and $\alpha = 1°$.

CONCLUSION :

In this paper, the convolution techniques have been used for reconstruction of the object having three regions of density variations; from parallel ray and fan-beam geometry using two types of filters. The differences between the reconstruction results using parallel ray and fan-beam were indistinguishable. Yet the speed advantage of collecting the data using the fan-beam was quite apparent for the larger data sets, which have wide applications in modern CT scanning systems.

The accuracy of reconstruction was improved with increasing the number of projections and making sample interval smaller. The reconstruction of the disk shows that, the first filter type has good results in variable density region; while the second type is good in the uniform region.

The used techniques can give better demonstration in case of using real CT projections due to realized acceptable accuracy.

REFRENCES :

1 . Bracewell, R.N., "Strip Integration in Radio-astronomy", Aust.J. Phys. 9, 198-217, 1956.
2 . Cormack, A.M., "Representation of a Function by its Line Integrals, with some Radiological Applications I", J.Appl. Phys. 34, 2722-2727, 1963.
3 . R.A. Crowther, D.J. Derosier, and A. Klug, "The Reconstruction of a Three-dimensional Microscopy" , Proc. Roy. Soc. London, Ser. A/317, pp. 319-340, 1970.
4 . G.N. Ramachandran and D.V. Lakshminarayanan, "Three-dimensional Reconstruction from Radiographs and Electron Micrographs :Application of Convolutions instead of Fourier Transforms", Proc. Nat. Acad. Sci. USA 68, 2236-2240, 1971 .
5 . L.A. Shepp and B.F. Logan, "Reconstructing Interior Head Tissuefrom X-ray Transmissions", IEEE Tran. Nucl. Sci. NS-21, 21-43, 1974.
6 . G.T. Herman, Ed., "Image Reconstruction from projections :Impelementation and Applications", Berlin Springer, 1979.
7 . R. Gordon, R. Bender, G.T. Herman, "Algebraic Reconstruction Technique (ART) for Three-dimensional Electron Microscopy and X-ray Photography", J. Theor. Biol. 29, 471-481, 19[illegible].
8 . G.N. Hounsfield, "Computerized Transverse Axial Scanning (Tomography) : Part I. Description of System", Br. J. Radiol. 46, 1016-1022, 1973.
9 . Brooks, R.A. and Di Chiro, G. "Theory of Image Reconstruction in Computed Tomography", Radiology 117, 561-572, 1972.
10. Robert, M. Lewitt, "Reconstruction Algorithms : Transform Methods", Proc. IEEE 71, 390-408, 1983.
11. Papoulis, "The Fourier Integral and its Applications", Mc Grow Hill Book Company, Inc. 1962.
12. Dreike, P. and Boyd, D.P., "Convolution Reconstruction of Fan-Beam Reconstructions", Comput. Graph Image Process.5, 459-469, 1976.
13. Petes, T.M. and Lewitt, R.M., "Computed Tomography with Fan-Beam Geometry", J. Comput. Assisted Tomography 1, 429-436, 1977.
14. Wang, L., "Cross-section Reconstruction with a Fan-Beam Scanning Geometry", IEEE Trans. Comput. C5, 264-268, 1977.

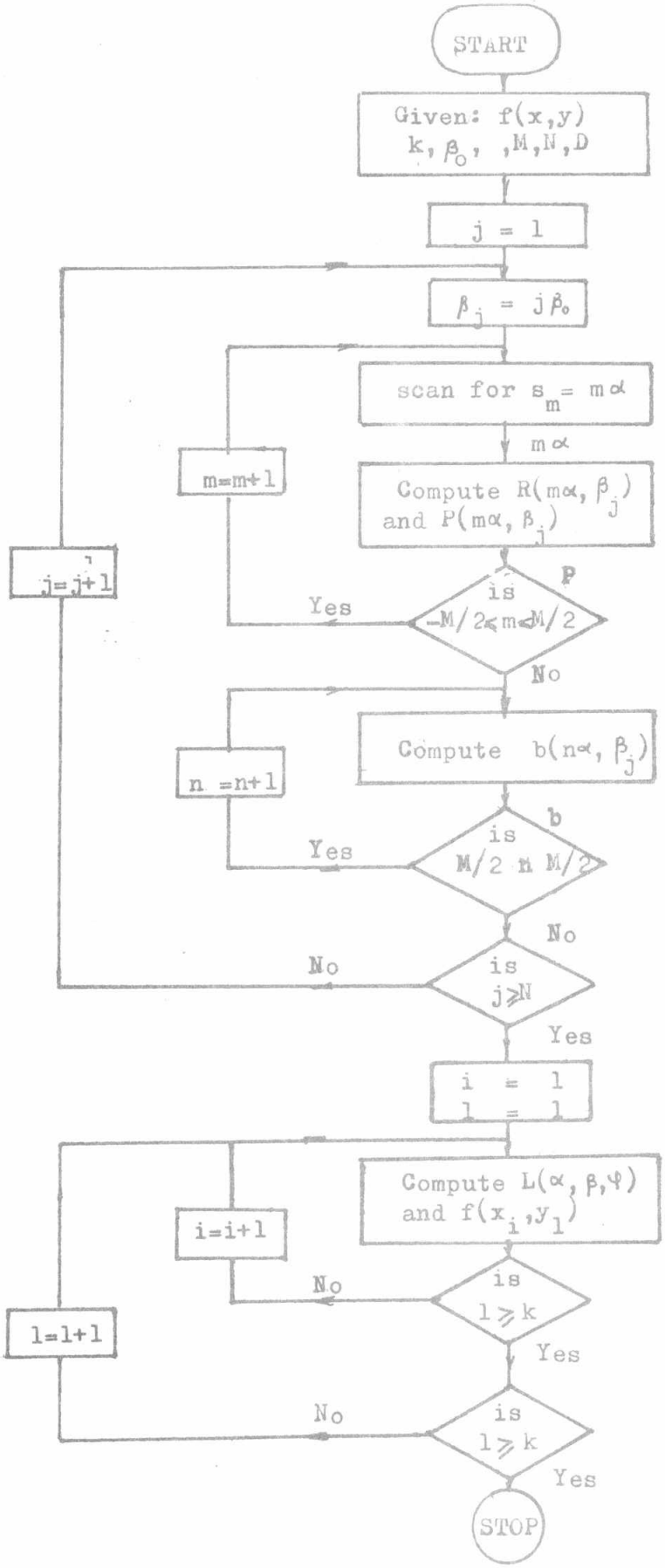

FIG. 4 Flowchart for Fan-beam reconstruction by convolution

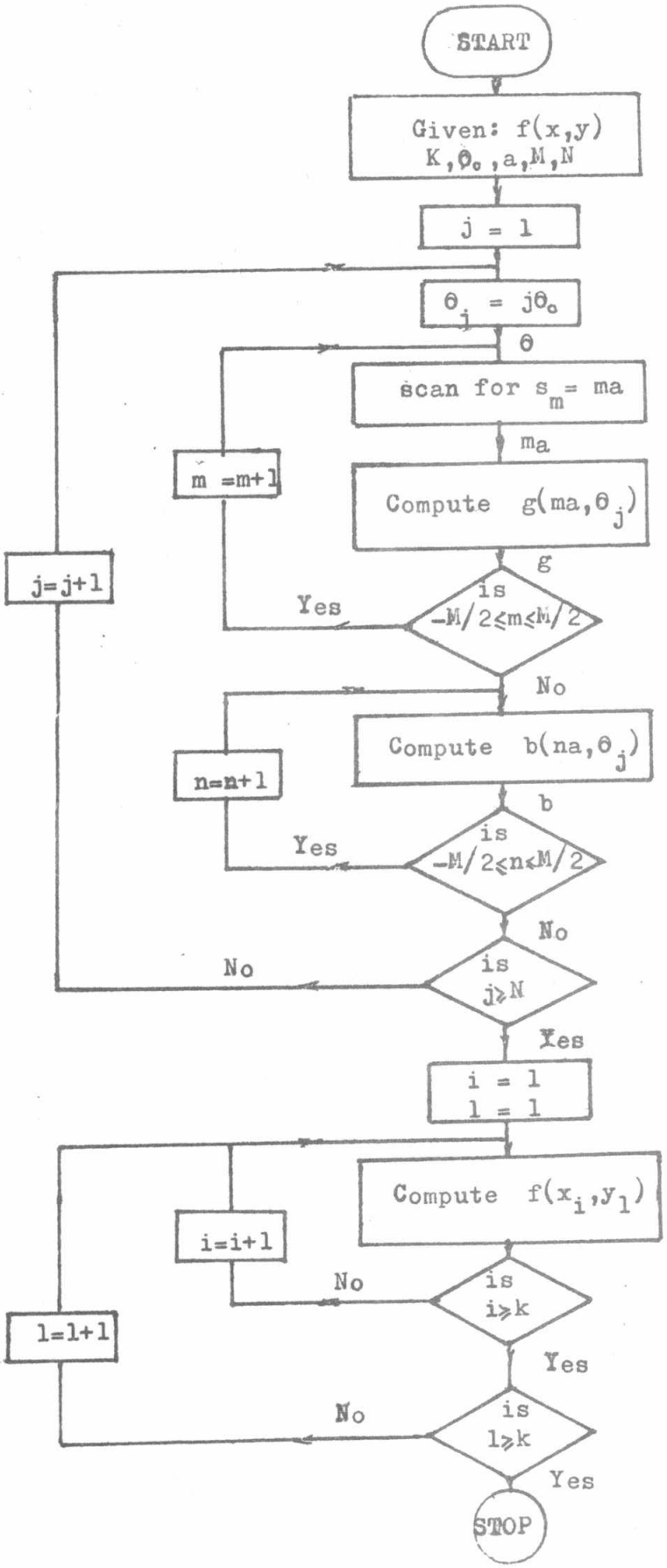

FIG. 3 Flowchart for parallel rays reconstruction by convolution